



Addition of V₂O₅-MnO₂/USY-zeolite catalyst in PTFE fiber for bag filter and its catalytic activity tests for NH₃-SCR at low-temperature



Jin Ho Boo ^{a,1}, Eunseok Kim ^{b,c,1}, Byung Chan Kwon ^d, Myung Jo Seo ^e, Ji-Man Kim ^c, Ji Bong Joo ^f, Dohyung Kang ^{g,*}, No-Kuk Park ^{d,*}

^a School of Chemical Engineering, Yeungnam University, 280 Daehak-ro, Gyeongsan, Gyeongbuk 38541, Korea

^b Heesung Catalysts Corp., 91 Somanggongwon-ro, Siheung-si, Gyeonggi-do 15088, Korea

^c Department of Chemistry, Sungkyunkwan University, 2066 Seobu-ro, Jangan-gu, Suwon-si, Gyeonggi-do 16419, Korea

^d Institute of Clean Technology, Yeungnam University, 280 Daehak-ro, Gyeongsan, Gyeongbuk 38541, Korea

^e Micro-one Inc. 368 Yeongok-road, Ibjang-myeon, Seobuk-gu, Cheonan-si, Chungnam 31026, Korea

^f Department of Chemical Engineering, Konkuk University, 120 Neungdong-ro, Gwangjin-gu, Seoul 05029, Korea

^g Department of Future Energy Convergence, Seoul National University of Science and Technology, 232, Gongneung-ro, Nowon-gu, Seoul 01811, Korea

ARTICLE INFO

Article history:

Received 9 December 2022

Revised 6 February 2023

Accepted 14 March 2023

Available online 23 March 2023

Keywords:

NO removal

NH₃-SCR

USY-zeolite

V₂O₅-MnO₂

PTFE fiber

ABSTRACT

This study investigated the catalytic activity of vanadium-manganese supported on USY-zeolite as a catalyst for low-temperature NO removal, and embedded the powder catalyst in PTFE filter of bag filter. The V₂O₅-MnO₂/USY-zeolite catalyst was prepared using the co-impregnation method, and the V₂O₅/MnO₂ ratio was 0/10, 2.5/7.5, 5/5, 7.5/2.5, or 10/0. The catalytic activity test for NH₃-SCR (selective catalytic reduction) of NO was performed at 150–230 °C. An enhanced NO conversion above 60% was exhibited in the low-temperature region below 230 °C, and the NO removal efficiency increased as the MnO₂ content increased. The NH₃-TPD and NO-TPD (Temperature Programmed Desorption) analysis confirmed that the NH₃ adsorption of the catalyst more significantly influences the NO removal performance than the NO adsorption. As the MnO₂ content on the catalysts increased, the strength and amount of adsorbed NH₃ increased, resulting in enhanced NO conversion. The catalyst-embedded PTFE (polytetrafluoroethylene) fiber was prepared by extruding physically mixed PTFE and catalyst powder. Scanning electron microscopy/energy dispersive X-ray spectroscopy confirmed that the catalyst was well dispersed on the surface and inside the PTFE fiber. The NO removal performance of the catalyst included PTFE fiber increased as the amount of the catalysts added was increased.

© 2023 The Korean Society of Industrial and Engineering Chemistry. Published by Elsevier B.V. All rights reserved.

Introduction

The use of fossil energy has increased the emission of nitrogen oxides and sulfur oxides, which cause ultrafine dust, into the atmosphere. The precursors of ultrafine dust are composed of nitrogen oxides, sulfur oxides, ammonia, volatile organic compounds, and heavy metals [1,2]. Air pollution gases are produced in large quantities in power generation industries, such as coal and natural gas power plants. Large-scale coal and natural gas power plants are equipped with the selective catalytic reduction (SCR) process and the flue-gas desulfurization (FGD) process to reduce nitrogen oxides

and sulfur oxide emissions and control the emission concentration according to air pollutant emission regulations [3–7]. Exhaust gas is discharged into the atmosphere after significant amounts of nitrogen oxides and sulfur oxides have been removed by the emission reduction technology. On the other hand, in small and medium-scale processes, where heating processes are being operated, there is still a shortage of facilities to remove nitrogen oxides. Indeed, the industrial sector has a significant amount of emissions [8–10].

Implementing air pollutant control technology in small and medium-scale processes is difficult because of the high capital and operating costs, limited site, and insufficient operational technology. In particular, in industrial facilities operating combustion and incinerators, the generation of thermal NO_x is inevitable during high-temperature combustion. In such a process, a facility for removing nitrogen oxides can be built using selective noncatalytic

* Corresponding authors.

E-mail addresses: dkang@seoultech.ac.kr (D. Kang), nokukpark@ynu.ac.kr (N.-K. Park).

¹ These authors contributed equally to this work.

reduction (SNCR) technology without using a catalyst. Because SNCR reduces nitrogen oxide by directly spraying ammonia or urea in a combustion furnace and an incinerator, there is no need for a separate catalytic process. Although SNCR technology is operated at temperatures above 900 °C, the reduction efficiency of nitrogen oxides is approximately 60%. Therefore, it cannot satisfy the strengthened air pollutant emission regulations [11–13]. Hybrid NO_x removal technology is being developed to actively respond to recently strengthened emission regulations [14–16]. Hybrid NO_x removal technology can link previously developed SNCR and SCR technologies. SCR technology reduces nitrogen oxides using a catalyst at 300 to 400 °C and removes nitrogen oxides emitted from power plants and internal combustion engine vehicles [17–20]. In the hybrid NO_x removal process, the level of nitrogen oxide removal can be further improved because nitrogen oxide is first reduced by SNCR technology, and secondary reduction is performed by SCR technology.

A honeycomb-type NO_x removal catalyst has been developed and used commercially in the SCR process [21–23]. A catalytic filter is additionally applied to remove low-concentration nitrogen oxides simultaneously with the dust removal. As the catalytic filter, the filter of ceramic and fabric material has been developed [24–32]. Considerable research has been conducted on catalytic filters because the NO removal efficiency can be improved by simply replacing the catalytic filter in the existing dust collection filter. However, adding high-activity catalyst powder into PTFE fibers still remains a challenge to be solved. Because the diluted exhaust gas including dust passes through a thin filter, the filter bag should filter out dust and reduce nitrogen oxide at low concentrations. Therefore, the activity of the catalyst must be high enough to reduce low-concentration nitrogen oxide. In addition, it must have low-temperature NO_x removal performance because the temperature in the dust collecting facility equipped with the filter bag is 150–230 °C. Furthermore, because the filter bag must periodically backwash the dust adhering to the outer wall of the filter, the catalyst must be strongly bonded with the filter so as not to be removed during the backwashing process. Thus, in this study, vanadium oxide and manganese oxide were used as active materials for the NO_x removal catalyst on a zeolite support with a high surface area to improve the low-temperature NO_x removal performance compared to the commercially used V₂O₅/TiO₂. Moreover, the catalyst powder was pre-mixed with PTFE fiber to be strongly entangled in the filter.

Although vanadium has been widely known as an active catalytic material for nitrogen oxide reduction, it has been reported that the reaction activity is high at a temperature above 250 °C [33–37]. On the other hand, manganese oxide was reported to have high activity in the low-temperature region of 150 °C or higher [38–42]. Nevertheless, manganese oxide is easily poisoned by sulfur oxides contained in the exhaust gas when used alone, and catalyst deactivation occurs [38,41,43]. In addition, ammonium salt is formed at low temperatures, and the catalytic activity is reduced

[44,45]. A previous study reported that the influence of sulfur oxide was improved using a combination of vanadium and manganese oxide [46–49].

This study examined the performance of the catalyst by changing the vanadium and manganese mixing ratio. USY-zeolite support with a high surface area was used to increase the removal efficiency of low-concentration NO. USY zeolite was relatively hydrophobic due to its high Si/Al ratio, which can minimize the effect of moisture in the exhaust gas. The prepared V₂O₅-MnO₂/USY-zeolite catalyst powder was mixed with PTFE powder, compressed, rolled, stretched, and slitted to prepare catalytic fiber materials, and their NO removal performances were tested at 200 °C. The prepared V₂O₅-MnO₂/USY-zeolite catalyst in PTFE fiber can be potentially used for the simultaneous removal of NO and dust.

Experiments

Preparation of catalysts

A V₂O₅-MnO₂/USY zeolite-based catalyst was prepared using the co-impregnation method. The loading of active material supported on the surface of the zeolite support was fixed at 10 wt. %, and the V₂O₅/MnO₂ content weight ratio was 0/10, 2.5/7.5, 5/5, 7.5/2.5, and 10/0. As shown in Fig. 1, a yellow color appeared as the vanadium content was increased, and a dark gray color was exhibited as the manganese content increased. USY-zeolite (Si/Al = 90) powder (Visionchemical Co.) was used as the support. Ammonium metavanadate (NH₄VO₃, Duksan Co.) and manganese nitrate solution (Mn(NO₃)₂, 50%, Duksan Co.) were used as precursors of the active materials V₂O₅ and MnO₂, respectively. The precursors were prepared as an aqueous solution and mixed. The precursor solution and zeolite powder were mixed in the round flask. A rotary vacuum evaporator slowly removed moisture to impregnate vanadium and manganese on the zeolite surface. The zeolite-based catalyst, in which the precursor was impregnated, was dried at 150 °C for 12 h in a dry oven and heat-treated at 400 °C for 4 h in a muffle furnace. The thermal-treated catalyst powder was named as V₂O₅(x)-MnO₂(10-x)/USY-zeolite. The catalyst finely pulverized by a ball mill was mixed with PTFE powder and used to prepare a PTFE-based catalytic fiber for use in a bag filter.

Preparation of PTFE-based catalytic fiber

The catalyst filter is manufactured as a bag filter by making a nonwoven fabric using PTFE fiber, a polymeric hydrophobic fiber. The PTFE-based catalytic fibers were prepared using the following procedure to add a powder-form catalyst in PTFE-based fibers. PTFE powder and V₂O₅-MnO₂/USY-zeolite prepared were physically mixed. The catalyst used for PTFE-based catalytic fiber is

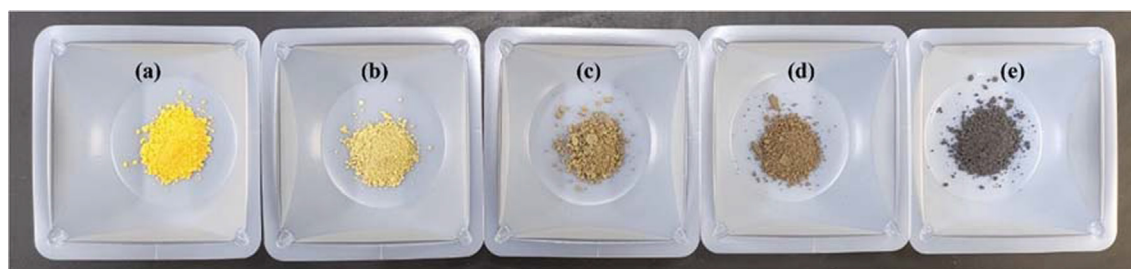


Fig. 1. Images of V₂O₅-MnO₂/USY-zeolite catalysts prepared using the impregnation method, (a) V₂O₅(10)/USY-zeolite, (b) V₂O₅(7.5)-MnO₂(2.5)/USY-zeolite, (c) V₂O₅(5.0)-MnO₂(5.0)/USY-zeolite, (d) V₂O₅(2.5)-MnO₂(7.5)/USY-zeolite, (e) MnO₂(10)/USY-zeolite.

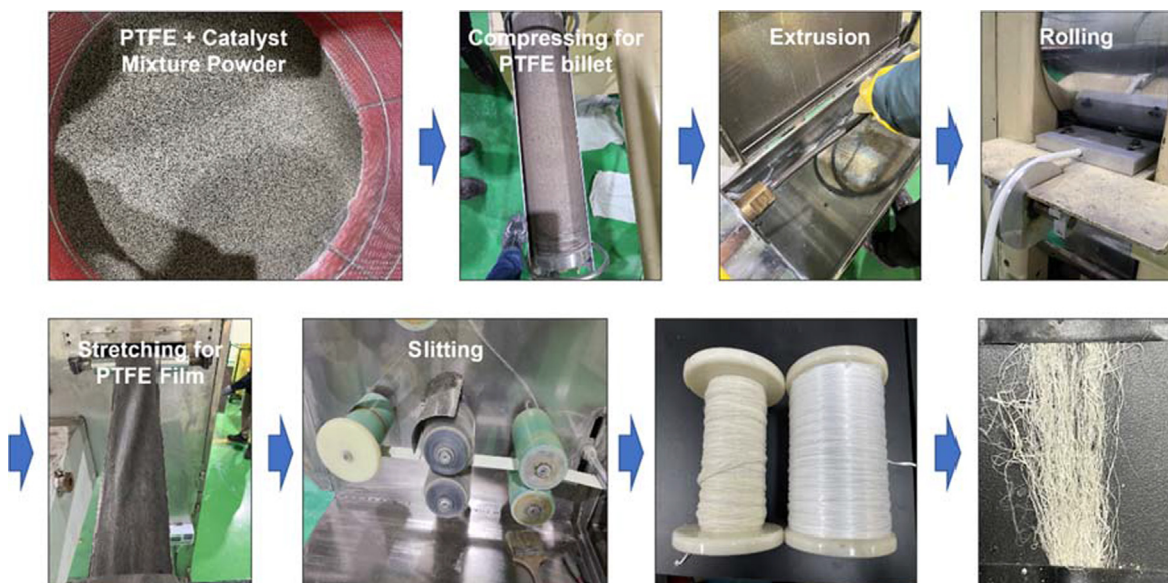


Fig. 2. Manufacturing procedure of the PTFE-based catalytic fiber.

$V_2O_5(2.5)$ - $MnO_2(7.5)$ /USY-zeolite. As shown in Fig. 2, the raw material mixed with PTFE and catalysts was made into a PTFE billet through a compression process, and the prepared PTFE billet was made into a thin PTFE rod using an extrusion method. After rolling and stretching into a PTFE film using a heated roller, the film was slitted to prepare a fiber-containing catalyst. A nonwoven fabric was prepared using the prepared PTFE fiber, and both sides of the fabric were laminated with a membrane filter to prepare a bag filter. In this study, the NO removal performance of the prepared PTFE fibers was evaluated. As shown in Fig. 3, three samples were prepared for the PTFE-based catalytic filter fibers according to the amount of catalyst added. The amount of catalyst was varied between 3, 4, and 5 wt. %. The fiber became dark gray as the amount of catalyst was increased.

Catalytic activity tests

As shown in Fig. 4, the activity of the NO removal catalysts prepared in this study was tested using a fixed-bed type catalytic reactor system. After packing the catalyst in the center of a tubular reactor, 170 ppmv nitrogen oxide was flowed, and ammonia gas corresponding to the stoichiometric ratio was then supplied to the catalytic reactor packed with catalysts for NH_3 -SCR. To investigate the sulfur tolerances of catalysts, NO reactant gas containing

20 ppmv of SO_2 was supplied to the catalysts. In addition, the effect of moisture in the reactant gas mixture was further examined by supplying NO reactant gas containing 2, 5, 8, and 10 vol% of moisture. In the catalytic reaction system, a 1/2-inch or 1.0-inch tubular reactor was installed in a vertical tube-type electric furnace, nitrogen oxide, nitrogen, and ammonia gas were connected to the front end of the reactor, and air was supplied using an air compressor. The gas inflow was controlled using a mass flow controller (MFC, Line Tech M3030V) for mixing these reaction gases, and a gas mixer was installed just before being supplied to the reactor to mix the simulated gas. In addition, to preheat the incoming gas, the gas supply line was heated to reaction temperature using a line heater. The catalyst bed temperature was measured by inserting a thermo-couple into the catalyst-packed bed in the reactor. A pressure gauge was installed at the top of the reactor to observe the pressure change in the reactor due to the packing of the powder catalyst. The reactor outlet was connected directly to a dedicated gas analyzer (Testo 350 K), and the nitrogen oxide concentration at the reactor outlet was measured before and after ammonia gas was introduced. The initial concentration of NO before the reaction was measured without passing through the catalyst bed by flowing the reaction gas through the by-pass line. The reaction temperature was adjusted to 150–230 °C, and the catalyst activity according to the temperature was measured. The performance of the powder catalyst was compared by charging the catalyst in a 1/2-inch tubular reactor, and the fibrous catalyst was charged in a 1.0-inch tubular reactor to compare the performance. The amount of the powder catalyst was approximately 0.51 g, and the fibrous catalyst was approximately 6.0 g. The space velocity (WHSV) was approximately 260,000 $mL \cdot g^{-1} \cdot h^{-1}$ based on the weight of the catalyst. The NO conversion and N_2 selectivity by the NH_3 -SCR reaction was calculated as in Equation (1) and Equation (2), respectively.

$$X_{NO}(\%) = \frac{C_{NO_x-input} - C_{NO_x-output}}{C_{NO_x-input}} \times 100 \quad (1)$$

$$S_{N_2}(\%) = 1 - \frac{2 \times C_{N_2O-output}}{C_{NO_x-input} + C_{NH_3-input} - C_{NO_x-output} - C_{NH_3-output}} \times 100 \quad (2)$$



Fig. 3. PTFE fibers prepared with different amounts of NO removal catalyst.

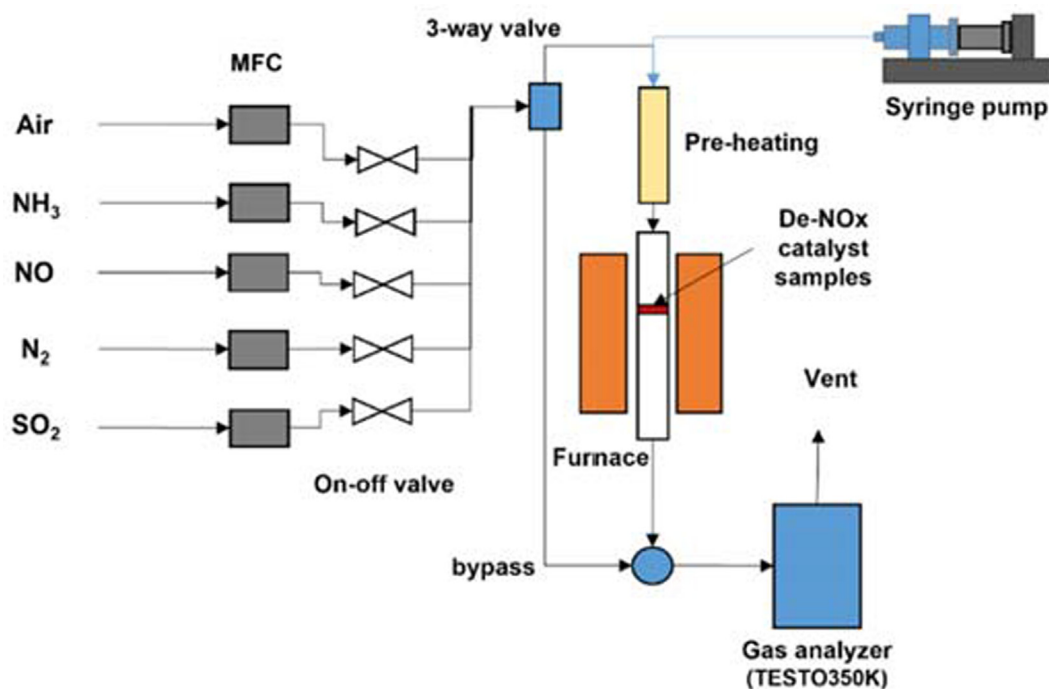


Fig. 4. Schematic diagram of the experimental apparatus for the catalytic activity tests by NH_3 -SCR.

X_{NO} : Conversion of NO

S_{N_2} : Selectivity of N_2

$C_{\text{NOx-input}}$: Concentration of NO flowing into catalytic reactor

$C_{\text{NOx-output}}$: Concentration of NO effluent from catalytic reactor

$C_{\text{NH}_3\text{-input}}$: Concentration of NH_3 flowing into catalytic reactor

$C_{\text{NH}_3\text{-output}}$: Concentration of NH_3 effluent from catalytic reactor

$C_{\text{N}_2\text{O-output}}$: Concentration of N_2O effluent from catalytic reactor

Characterization of the catalysts

The surface area, pore volume, and pore size of the catalyst supporting vanadium and manganese on the surface of the hydrophobic zeolite were measured using the N_2 adsorption method (Micromeritics, 3-Flex). Samples were degassed at 200 °C under vacuum before measuring N_2 adsorption–desorption isotherms. In addition, the crystal structure of the catalytic active material supported on the zeolite support was analyzed by X-ray diffraction (XRD, DIAOME, MOD for bulk (powder)). The binding energy spectrum of V and Mn was analyzed by X-ray photoelectron spectroscopy (XPS, ThermoScientific Co., K-Alpha) to confirm the oxidation states of trace amounts of catalytic active material not confirmed by XRD. NH_3 and NO TPD tests (BEL Japan Inc., BELCAT II) were performed to observe the adsorption and desorption behavior of NH_3 and NO of the prepared catalyst. The NH_3 -TPD and NO-TPD tests were performed as follows. The catalyst was charged in the reactor chamber for the TPD experiment, purged while flowing with argon gas at 300 °C for 2 h, and approximately 1 vol% of NO gas or 5 vol% of NH_3 gas with an argon balance at room temperature. After adsorbing the adsorbed gas to the catalyst while flowing, the desorption amount was measured while the temperature was increased from room temperature to 900 °C at a rate of 10 °C/min. The surface morphology of the PTFE fiber was observed by scanning electron microscopy (FE-SEM/EDS(3), HITACHI, Ltd, S-4800), and the distribution of V, Mn, Si, and Al on the surface and inside of the PTFE fiber was observed by energy dispersive X-ray spectroscopy (EDX) mapping. Thermogravimetric analysis (TGA, Scinco TGA N-1000/1500) was performed to quanti-

tatively measure the amount of catalyst contained in the PTFE-based catalytic fiber.

Results and discussion

N_2 -adsorption analysis

The surface area, pore volume, and pore size of the five zeolite-supported catalysts with controlled vanadium and manganese contents prepared in this study were measured using a nitrogen-adsorption method. As shown in Table 1, the catalyst had a large surface area of approximately 681 to 715 $\text{m}^2\cdot\text{g}^{-1}$, and the case where only vanadium or manganese was supported showed a relatively low surface area. However, no significant surface area change was observed because the same zeolite support was used in the catalysts. The pore volume and mean pore size were 0.19 to 0.22 $\text{cm}^3\cdot\text{g}^{-1}$ and 4.6 to 5.2 nm, respectively. No significant change was observed because the total amount of vanadium and manganese supported on the zeolite support was maintained at approximately 10 wt.%.

XRD analysis

XRD analysis was performed to confirm the crystal structures of the vanadium and manganese catalysts supported on the powder catalyst; Fig. 5 shows the XRD patterns of each catalyst. The XRD pattern showed a strong diffraction pattern of the zeolite used as a support, with low intensities peaks of V_2O_5 and MnO_2 . Nevertheless, the characteristic MnO_2 -related XRD peaks of the MnO_2/USY -zeolite catalyst were observed at 28°, 38°, 44°, 56°, and 59° 2 θ [50,51]. On the other hand, a peak capable of identifying vanadium could not be confirmed, suggesting that the small amounts of active catalytic metals were highly dispersed over the high surface of the zeolite. Because XRD could hardly detect the crystallinity of active metals, the crystal structure could not be specified, and the change in the oxidation state of vanadium and manganese into a composite oxide could not be observed.

Table 1
Surface area, pore volume, and pore size of V₂O₅-MnO₂/USY-zeolite catalysts measured by the N₂-adsorption method.

| Catalysts | Surface area, m ² ·g ⁻¹ | Total pore volume, cm ³ ·g ⁻¹ | Mean pore size, nm |
|--|---|---|--------------------|
| V ₂ O ₅ (10)/USY-zeolite | 681.1 | 0.22 | 5.2 |
| V ₂ O ₅ (7.5)-MnO ₂ (2.5)/USY-zeolite | 715.2 | 0.23 | 4.9 |
| V ₂ O ₅ (5.0)-MnO ₂ (5.0)/USY-zeolite | 711.0 | 0.19 | 5.2 |
| V ₂ O ₅ (2.5)-MnO ₂ (7.5)/USY-zeolite | 705.1 | 0.19 | 4.9 |
| MnO ₂ (10)/USY-zeolite | 681.2 | 0.19 | 4.6 |

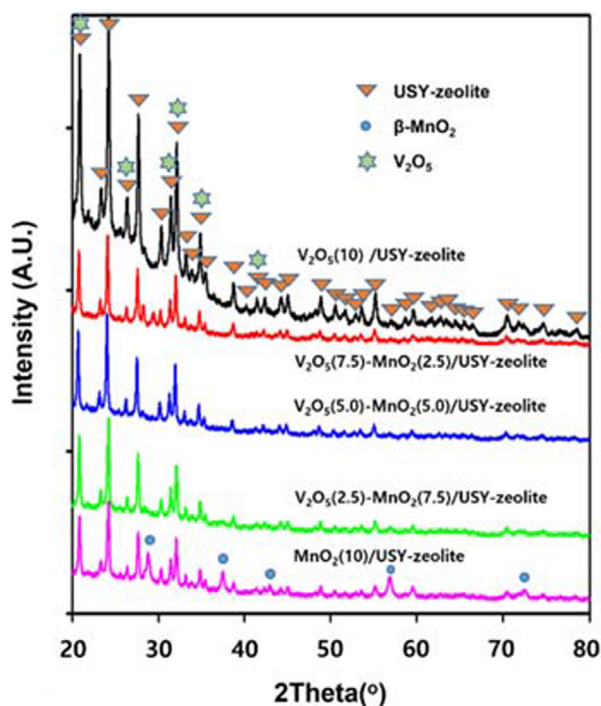


Fig. 5. XRD patterns of V₂O₅-MnO₂/USY-zeolite catalysts.

XPS analysis

XPS was performed to investigate the oxidation state of active metal oxides in the catalysts [52–55]. Fig. 6 presents the XPS analysis results of V2p, Mn2p, and O1s. Fig. 6(a) showed typical binding energy spectra of V₂O₅. The binding energy of Vp_{3/2} and Vp_{1/2} was confirmed at 516.8 eV and 524.3 eV, which corresponded to the binding energy of V₂O₅ [52,53]. The peak intensity decreased with decreasing the amount of V in catalysts. In addition, no shift in V2p binding energy was observed, suggesting a V-Mn composite oxide was hardly formed. Reddy et al. reported that when vanadium oxide is mixed with an additive, a composite metal oxide is formed in the calcination process above 700 °C, thereby shifting the binding energy [52]. On the other hand, the binding energy of Mn2p_{3/2} and Mn2p_{1/2} appeared at 641.8–642.3 eV and 653.4–654.1 eV, respectively (Fig. 6(b)), which is the XPS spectrum for Mn₂O₃ and MnO₂; hence MnO₂ and Mn₂O₃ coexisted [54,55]. In the XPS spectrum of Fig. 6(c), the small peak of O1s binding energy at 529 eV can be seen as the binding energy of Mn–O bonding of MnO₂, and the peak at 530 eV is the O1s spectrum corresponding to V–O of V₂O₅. [53,55]. As the amount of Mn increased in the catalyst, the small peak shifted from 530 eV (V–O) to 529 eV (Mn–O). The strong peak at a binding energy of 532.5 eV is the spectrum of O1s corresponding to the Al–O and Si–O bonds in the zeolite structure [56–59].

NH₃-TPD analysis

NH₃-TPD tests were performed to investigate the adsorption properties of NH₃ for the five catalysts prepared in this study. As shown in Fig. 7, the NH₃ desorption behaviors of the five catalysts showed significant differences. A comparison of the desorption behavior of NH₃ in the range of 100–250 °C showed that the amount of NH₃ desorption increased as the V₂O₅ content was increased. On the other hand, the amount of NH₃ desorption in the range of 250–500 °C increased as the content of MnO₂ increased. Furthermore, the NH₃ desorption amount in the range of 500–900 °C also increased with increasing MnO₂ content. Based on these results, as vanadium content increased, most of the NH₃ is desorbed in the low-temperature region below 250 °C. On the other hand, as the MnO₂ content increased, the desorption of NH₃ decreased below 250 °C and the desorption increased above 250 °C. The strong adsorption sites which desorb NH₃ above 250 °C were more related to the NH₃-SCR reaction. Therefore, the NO removal performance in the low-temperature NH₃-SCR reaction is improved by increasing the MnO₂ content due to the high adsorption amount of strongly adsorbed NH₃ as a reducing agent of NO. It has been well known that the desorption of NH₃ in the range of 100–200 °C corresponds to the weak Bronsted acid sites, and the desorption in the range of 300–400 °C corresponds to the Lewis acid sites [60–62]. Wang et al. [60] reported that the NO_x conversion is directly related to Lewis acid site of the Ce/TiO₂ catalyst. Although new adsorption sites of NO_x were generated by adding alkali metals (Na, K) to the catalyst, weakening of Lewis acid sites was observed in the NH₃-TPD profile, resulting in the decrease of the catalytic activity for the SCR reaction. Liu et al. [61] reported that desorption peaks by NH₄⁺ bonded to strong Bronsted acid sites and Lewis acid sites and coordinated NH₃ at temperatures above 200 °C on FeTiO_x and TiO₂ catalysts affected the high denitrification performance of the catalysts. Li et al. [62] have confirmed that a high-temperature NH₃ desorption peak above 300 °C in the NH₃-TPD experiment of the MnO₂-Nb/TiO₂ catalyst was mainly attributed to its enhanced catalytic activity for SCR reaction. Among the V₂O₅-MnO₂/USY-zeolite catalysts prepared in this study, the adsorption of coordinated NH₃ bound to the Lewis acid sites increased as the content of MnO₂ increased.

NO-TPD analysis

NO-TPD tests were performed over five catalysts to observe the adsorption/desorption behavior of NO, the reactant of the SCR reaction. As shown in Fig. 8, the desorption of NO adsorbed on the catalysts in NO-TPD tests showed a significantly different trend compared to the NH₃-TPD tests. A large amount of NO was desorbed in the high-temperature region, and there was no difference in the low-temperature region. Nevertheless, the desorption amount of NO was relatively higher when manganese was added to the catalyst than that of only V₂O₅ in the 100 to 400 °C. In particular, the desorption amount of adsorbed NO was highest when manganese and vanadium were supported at a ratio of 5:5 in the low-temperature region. On the other hand, most of the adsorbed

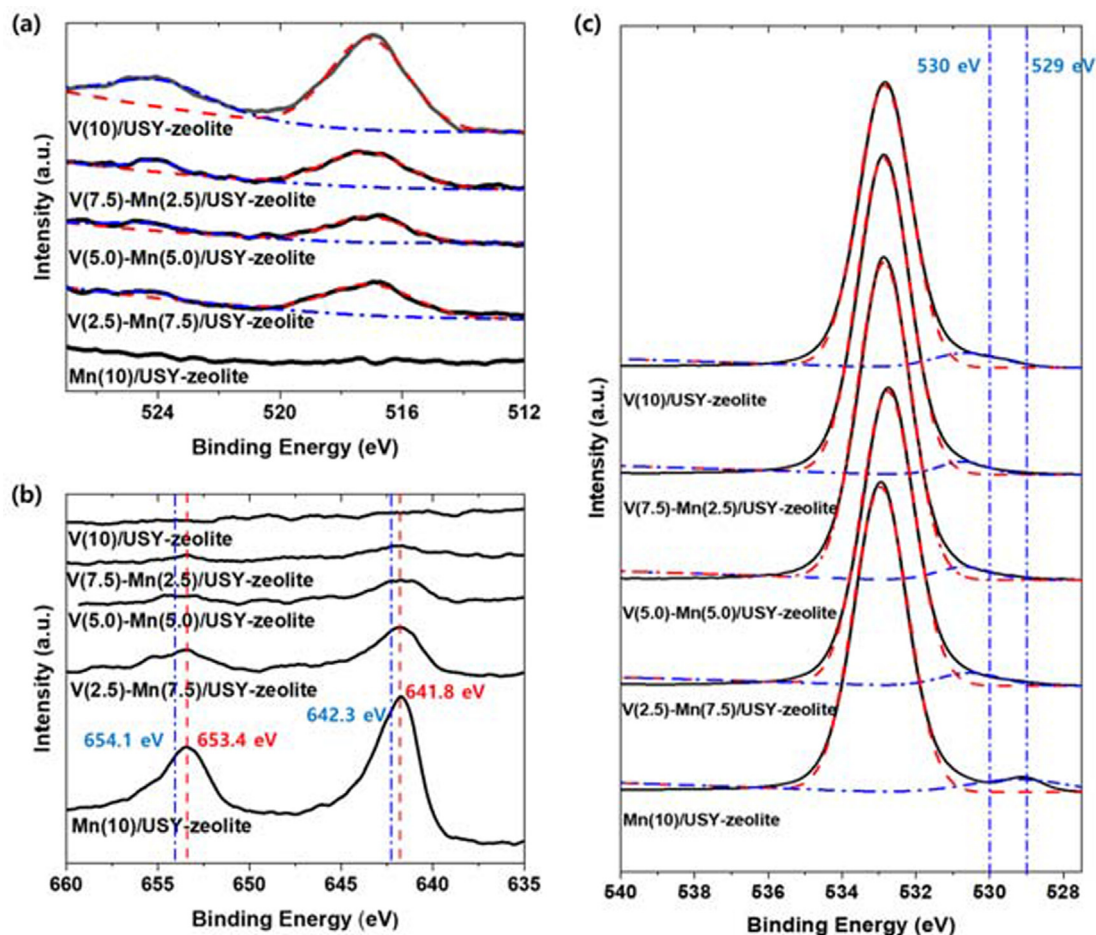


Fig. 6. XPS results of V_2O_5 - MnO_2 /USY zeolite catalysts, (a) V2p, (b) Mn2p, (c) O1s.

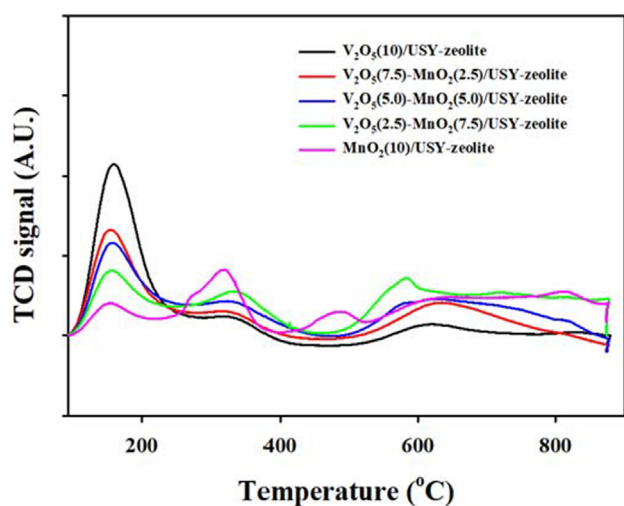


Fig. 7. NH_3 -TPD diagram over the V_2O_5 - MnO_2 /USY zeolite-based catalysts.

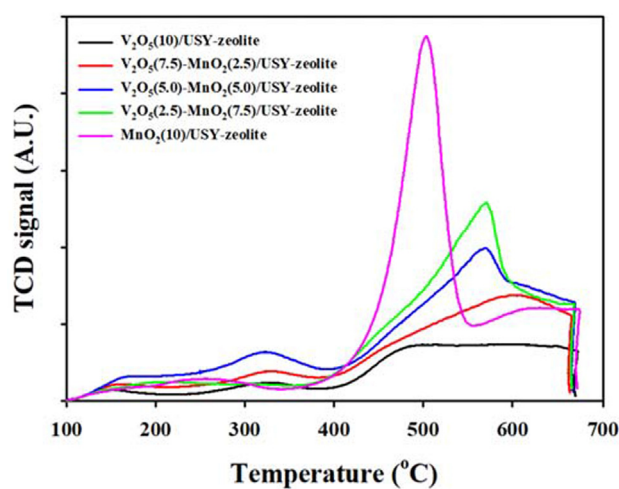


Fig. 8. NO -TPD diagram over V_2O_5 - MnO_2 /USY zeolite-based catalysts.

NO was desorbed above $400\text{ }^\circ\text{C}$, and the desorption amount of NO increased as the MnO_2 content was increased. However, the adsorption strength was maximized when the V:Mn ratio was 2.5:7.5. When considering the NO adsorption amount and strength together, V(2.5)-Mn(7.5)/USY-zeolite was selected as the potentially optimized catalyst. When it was considered that all five catalysts have strong adsorption capacity for NO , the adsorption of NO

does not make a significant difference in catalytic activity, but rather the adsorption of NH_3 determines the overall activity.

Catalytic activity analysis

The activity of the powder catalysts on the NH_3 -SCR reaction was compared by measuring the NO removal performance over five catalysts by changing the reaction temperature. As shown in

Fig. 9, the NO conversion increased as the reaction temperature increased. In addition, the NO conversion also showed a significant difference according to the composition of the catalyst at each

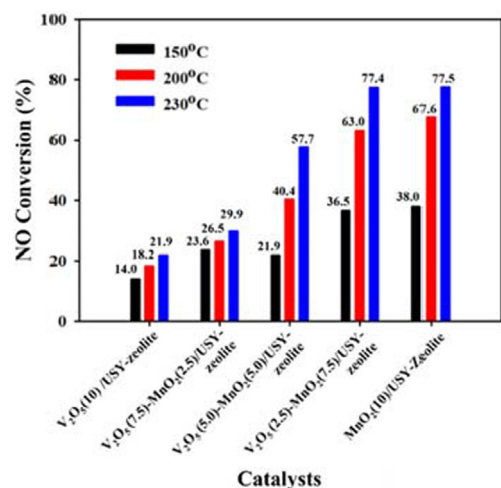
reaction temperature. The V_2O_5/USY -zeolite catalyst showed NO conversion of 14.0%, 18.2%, and 21.9% at 150, 200, and 230 °C, respectively. The $V_2O_5(7.5)-MnO_2(2.5)/USY$ -zeolite catalyst exhibited NO conversions of 23.6%, 26.5%, and 29.9% at 150, 200, and 230 °C, respectively, indicating a higher NO conversion than the catalyst only impregnated with V_2O_5 . The $V_2O_5(5.0)-MnO_2(5.0)/USY$ -zeolite catalyst showed a higher NO conversion under the same temperature conditions than the catalyst only impregnated with V_2O_5 . In particular, a sharp increase in the NO conversion above 200 °C was observed. The $V_2O_5(2.5)-MnO_2(7.5)/USY$ -zeolite and $MnO_2(10)/USY$ -zeolite catalysts exhibited a similar level of NO conversion under the same temperature condition, and a high NO conversion of above 63% was indicated. These catalysts exhibited a NO conversion of approximately 77% at a reaction temperature of 230 °C. In addition, the catalyst produced approximately 38% NO conversion, even at a low temperature of 150 °C. Zhang et al. [63] reported the generation of NO_2 and N_2O by oxidation of NO and NH_3 , respectively, on Mn-based catalysts during the SCR reaction. The concentration of NO_2 and N_2O in the outlet of the catalytic reactor increased as the reaction temperature increased due to the promoted oxidation of NO and NH_3 . The oxidation reactions and resulting NO_2 and N_2O generation were significantly dependent on the composition of the support. In this study, NO_2 was hardly detected during the NH_3 -SCR reaction of NO. Even if the small amount of NO_2 was produced by MnO_2 , the generated NO_2 might be rapidly reduced into N_2 by NH_3 on the catalysts. According to the Langmuir-Hinshelwood mechanism for the NH_3 -SCR reaction proposed by Li et al. [62], the adsorbed NO_2 is reduced to N_2 by the reaction with nearby adsorbed NH_3 on the catalyst before being desorbed. Therefore, gas-phase NO_2 may not be detected under the reaction conditions conducted in this study.

As shown in Fig. 9(b), a negligible level of N_2O was detected at 150 °C. However, it increased to almost 4 ppmv at 200 °C, and 18 ppmv at 230 °C. As reported by Zhang et al. [63], the concentration of N_2O increased as the reaction temperature increased. The five catalysts prepared in this study showed the same tendency, and the catalyst with a high amount of MnO_2 , showed a relatively greater increase of N_2O by NH_3 oxidation. Yao et al. [64] reported that the exhaust of N_2O by NH_3 -SCR reaction on a MnO_2 -based catalyst was greatly influenced by the type of support.

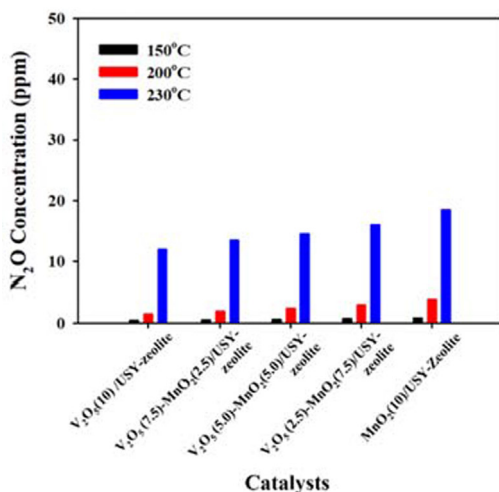
The N_2 selectivity was maintained above 97% on all $V_2O_5-MnO_2/USY$ -zeolite catalysts in the NH_3 -SCR reaction below 200 °C, and decreased in the range of 87–94% at 230 °C due to the generation of N_2O . Among the catalysts prepared in this study, higher N_2 selectivity was obtained on the $V_2O_5(2.5)-MnO_2(7.5)/USY$ -zeolite catalyst.

The catalytic activity at a low temperature below 230 °C was high with a higher MnO_2 content. The catalytic activity of the NO removal reaction depends on the adsorption strength of NH_3 and NO over the catalyst surface. Although the NO-TPD showed different adsorption strengths depending on the composition of the catalysts, NO molecules adsorbed on catalysts were hardly desorbed from 100 to 400 °C. However, the strength of NH_3 adsorption varied among catalysts in this temperature range. Therefore, the NH_3 adsorption had a dominant effect on the reaction rate for NH_3 -SCR reaction when comparing the adsorption strength of NO in the temperature range below 230 °C.

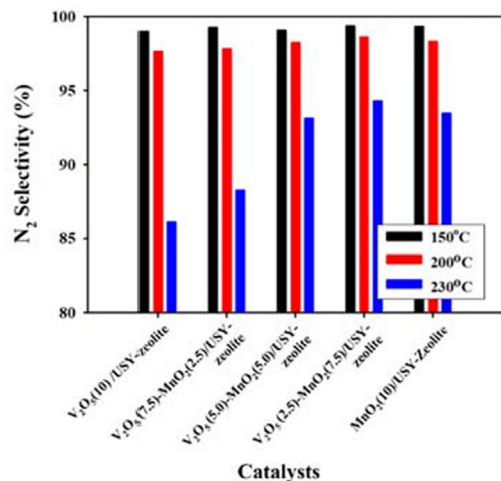
To investigate the catalytic activities inhibited in the presence of SO_2 , approximately 20 ppmv of SO_2 was mixed in the reaction gas. Other compositions of reactant gas introduced into the reactor was kept same except for adding SO_2 . As shown in Fig. 10(a), the initial NO concentration (170 ppmv) decreased by SCR reaction as soon as NH_3 was supplied into the catalyst, but the NO concentration increased with the introduction of SO_2 . From results, the NO conversion of the catalyst in the presence of SO_2 was plotted versus the time in Fig. 10(b). In the case of $MnO_2(10)/USY$ -zeolite, the NO



(a)

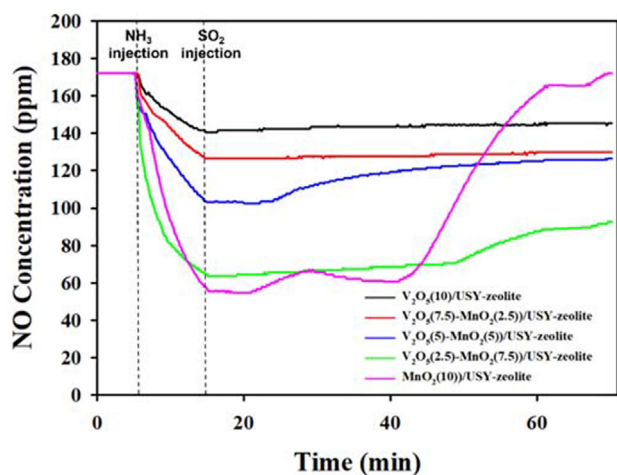


(b)

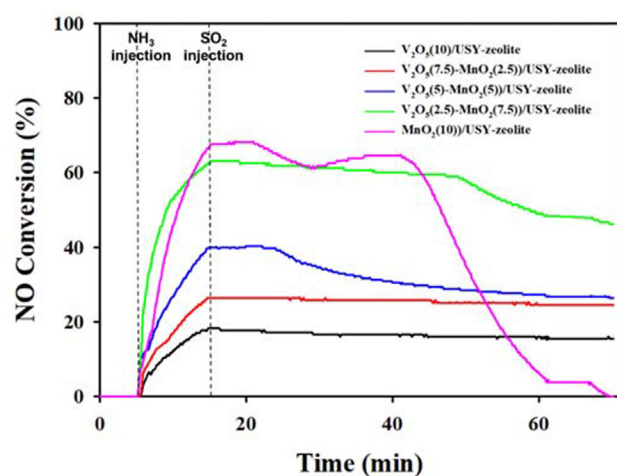


(c)

Fig. 9. Catalytic activity tests over $V_2O_5-MnO_2/USY$ -zeolite catalysts for SCR, (a) NO conversion, (b) N_2O concentration, (c) N_2 selectivity.



(a)



(b)

Fig. 10. NO concentration versus time and (b) NO conversion versus time over V_2O_5 - MnO_2 /USY-zeolite in the presence of 20 ppmv SO_2 at 200 °C.

conversion of approximately 60–70% was initially maintained even in the presence of SO_2 . However, the NO conversion rapidly decreased to 5%, 30 min after SO_2 was introduced. On the other hands, about 60% of the initial NO conversion of $V_2O_5(2.5)$ - $MnO_2(7.5)$ /USY-zeolite was gradually decreased without showing sharp decrease even in the presence of SO_2 . For remaining catalysts, although the decrease of NO conversions by SO_2 were insignificant, their catalytic activities were much lower than those of $MnO_2(10)$ /USY-zeolite and $V_2O_5(2.5)$ - $MnO_2(7.5)$ /USY-zeolite in the presence of SO_2 . Overall, the NO conversion increased with the increase of MnO_2 content in the catalyst under NO- NH_3 - SO_2 mixed flow, but $MnO_2(10)$ /USY-zeolite showed the significant deactivation by SO_2 . Zhang et al. [65] reported the effect of SO_2 is insignificant when the desulfurization process is installed in the up-stream of NH_3 -SCR process. However, low-concentration SO_2 might be introduced into NH_3 -SCR process even after the desulfurization process. Thus, although the catalysts with high MnO_2 content show high activity for NH_3 -SCR reaction at low temperature, V_2O_5 should be mixed with MnO_2 to minimize the catalytic deactivation by SO_2 . In this study, $V_2O_5(2.5)$ - $MnO_2(7.5)$ /USY-zeolite was chosen as the optimized catalyst for NH_3 -SCR process.

Wet NO- NH_3 mixture gas containing 2, 5, 8, and 10 vol% of steam was injected into the catalyst to examine the effect of moisture on the catalytic activity for NH_3 -SCR reaction, as shown in Fig. 11. A slight decrease in NO conversion was observed as the moisture increased in the reaction gas mixture. As the MnO_2 content increased in the catalyst, its catalytic activity was less affected by moisture. Zhang et al. [65] added 10 wt.% of hydrophobic PTFE into the SCR catalyst to hinder the deactivation of MnO_2 catalyst by moisture in the exhaust gas. In this study, because hydrophobic USY-zeolite was used as the support, the water-resistance of V_2O_5 - MnO_2 -based catalyst can be enhanced.

SEM analysis

When considering the catalytic activity and the potential sulfur and water resistance together, $V_2O_5(2.5)$ - $MnO_2(7.5)$ /USY-zeolite was selected as the optimum catalyst. Therefore, the catalytic PTFE fiber was prepared using $V_2O_5(2.5)$ - $MnO_2(7.5)$ /USY-zeolite. The surface morphology of PTFE fibers containing $V_2O_5(2.5)$ - $MnO_2(7.5)$ /USY-zeolite catalyst was observed by SEM. As shown in Fig. 12, the catalyst particles were dispersed uniformly on the surface of the PTFE fibers. In the process of manufacturing the PTFE-based catalytic fibers, the amount of catalyst mixed in the fiber was varied to approximately 3.0, 4.0, and 5.0 wt. %. The size of the catalyst particles observed by SEM was mostly less than 1.0 μm , and relatively uniform particles were distributed. Particles larger than 2.0 μm were also partially observed, but they were not distributed at a level to be representative. A large amount of catalyst was distributed in the valleys formed in the longitudinal direction on the PTFE fibers. As shown in Fig. 12(a)–(c), the valleys containing many catalyst particles were formed during the stretching process of PTFE film. Most of the catalyst was entangled present inside the polymer fiber when the fiber was manufactured by mixing the polymer material PTFE and the solid inorganic catalyst. The catalyst particles exposed to the outer surface of the fiber can only be used as an active catalyst site. Therefore, the activity of the catalytic PTFE fiber can be lower than powder catalysts.

As shown in Fig. 13, PTFE fibers were prepared by the following procedures; (1) physically mixing PTFE powder and catalyst powder, (2) compression of the PTFE-catalyst mixture powder, (3) production of a PTFE rod in which the catalyst was dispersed by hot extrusion, (4) formation of a PTFE film by hot rolling, (5) stretching of the PTFE film, (6) slitting of stretched thin PTFE films to foam the fiber. Here, the physically mixed PTFE and catalyst powder was

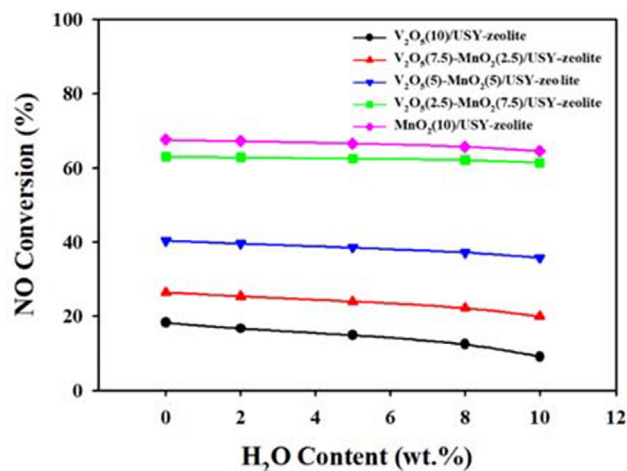


Fig. 11. NO conversion versus time over V_2O_5 - MnO_2 /USY-zeolite in the presence of moisture at 200 °C.

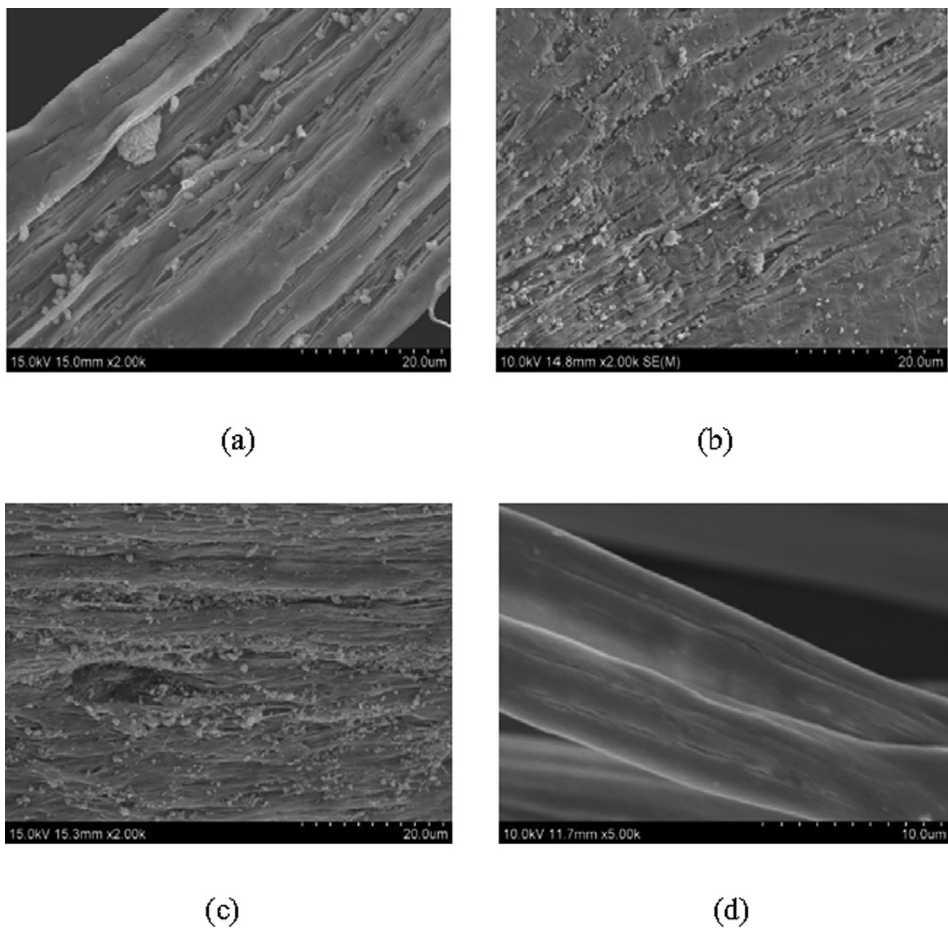


Fig. 12. SEM images of surface morphology over PTFE-based catalytic fibers prepared by mixing various amounts of $V_2O_5(2.5)\text{-MnO}_2(7.5)/\text{USY-zeolite}$, (a) 3.0 wt. %, (b) 4.0 wt. %, (c) 5.0 wt. %, (d) catalyst free PTFE fiber.

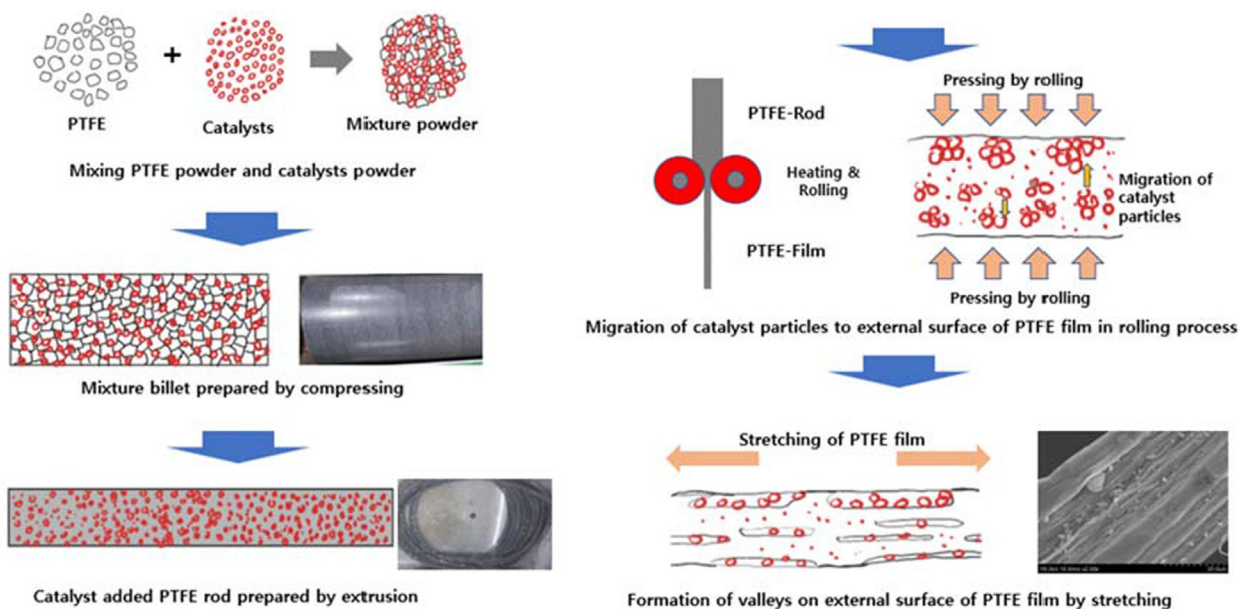


Fig. 13. Schematic diagram of the surface modification of catalytic PTFE.

compressed to form a cylindrical product having 100 mm of diameter and 300 mm of length. In the hot extrusion step, a long PTFE rod having high density and flexibility was manufactured by the

extrusion of PTFE billet and the catalyst was homogeneously dispersed inside the PTFE rod. The catalyst-contained PTFE rod was again passed between two heated rolls to produce a PTFE film. In

this step, the pressure was applied in the vertical direction of the rod and therefore, the catalyst particles migrated toward the outside surface of the film. During the stretching process, the PTFE film was pulled in the longitudinal direction, and valleys were formed on the external surface of the PTFE film. A large amount of the catalyst was present in the valleys formed on the surface of the PTFE fibers, which can enhance the activity of the catalytic PTFE fiber. On the other hand, the catalyst-free PTFE fibers prepared using the same method showed no valleys, as shown in Fig. 12(a).

EDX analysis

The distribution of catalyst particles on the cross-section of the PTFE fiber was examined. A knife cut the PTFE fibers after freezing with liquid nitrogen, and their cross-section was observed using the EDX mapping technique. Although the catalyst content in the PTFE fiber was approximately 3.9–5.0 wt. %, the total amount of V and Mn supported on the catalyst was less than 10 wt. %. Thus, the maximum Mn and V content was approximately 0.5 wt. % on the PTFE fiber. Due to the low Mn and V contents in the fiber, the distribution of catalyst could not be clearly observed with their images. It was effective to observe the dispersion of the catalyst inside the PTFE using the mapping image of Si and Al with the

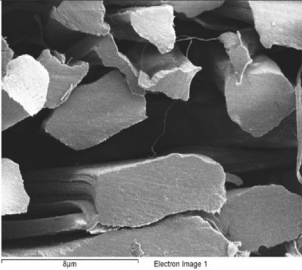
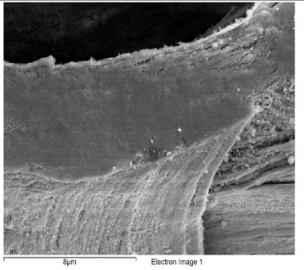
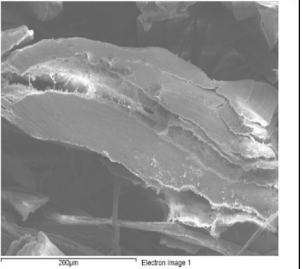
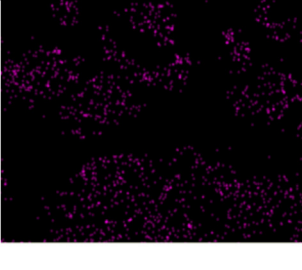
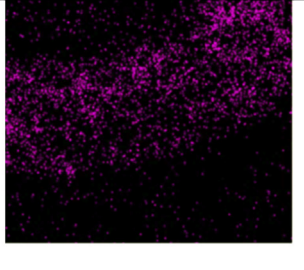
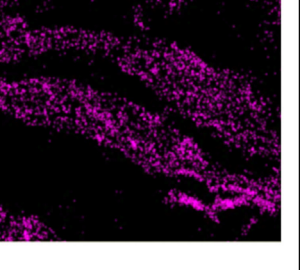
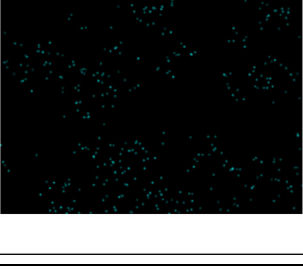
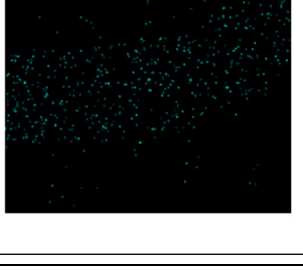
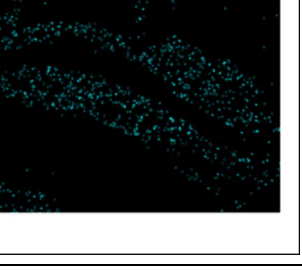
highest content. As shown in Table 2, the image of Si and Al on the inside cross-section of PTFE fibers was brighter with an increasing amount of catalyst added in the PTFE fiber. The relatively large catalyst particles observed on the surface of the PTFE fiber (Fig. 12) were not observed in the cross-section, and it appeared that more catalyst was distributed on the fiber surface.

Activity tests of PTFE fiber with the addition of catalyst

The catalytic activity of PTFE catalytic fibers containing $V_2O_5(2.5)$ - $MnO_2(7.5)$ /USY-zeolite catalysts of 3, 4, and 5 wt. % were investigated by NH_3 -SCR reaction. As the condition for the catalytic activity, 6.0 g of PTFE catalytic fibers were packed into the 1-inch tubular reactor. The NO concentration in a simulated exhaust gas was approximately 170 ppmv, and the reactant gas was supplied to the reactor at a flow rate of 1.5 L/min. The reaction temperature was maintained at 200 °C. The NO conversion obtained by the catalytic activity tests in the fixed-bed reactor system increased as the amount of catalysts added to the fiber increased, as shown in Fig. 14. The NO conversion over the PTFE catalytic fiber prepared with 3.0, 4.0, and 5.0 wt. % of $V_2O_5(2.5)$ - $MnO_2(7.5)$ /USY-zeolite catalysts was 8.3, 11.2, and 14.2%, respectively.

The actual catalyst content of the PTFE catalytic fiber prepared by adding the catalyst was measured by TGA. The PTFE catalytic

Table 2
Cross-section images of $V_2O_5(2.5)$ - $MnO_2(7.5)$ /USY-zeolite-added PTFE fiber by SEM and EDX mapping.

| Amount of catalysts | 3.0 wt. % | 4.0 wt. % | 5.0 wt. % |
|---------------------|---|---|--|
| SEM images |  |  |  |
| Si mapping |  |  |  |
| Al mapping |  |  |  |

fiber samples were oxidized in air at a heating rate of 5 °C/min from room temperature to 900 °C, and the weight change was observed. As shown in Fig. 15, the weight loss was confirmed at 400 °C for all three samples, and PTFE was completely oxidized at 580 °C. A difference in the residual weight was observed after complete oxidation depending on the amount of catalyst added in PTFE. After oxidation of PTFE catalytic fibers, the residual amounts prepared with 3, 4, and 5 wt. % catalysts were 1.29%, 1.88%, and 2.18% of the initial weight, i.e., the actual content of the catalyst contained in the three PTFE catalytic fiber samples. Only approximately 43% of the amount of catalyst added in the manufacturing process of the PTFE catalytic fiber was present in the PTFE fiber. Therefore, approximately 57% of the catalyst was lost during the slitting process when manufacturing PTFE film into a fiber.

Based on TGA results, the NO removal performance of PTFE fiber was compared with a powder catalyst corresponding to the amount of catalyst contained in the PTFE catalytic fiber. As shown in Fig. 16, when the powder catalyst was charged corresponding to the 1 wt. % catalyst in the PTFE fibers, the NO conversion was maintained at approximately 15%, and a NO conversion of approximately 22% was obtained when the powder catalyst corresponding to the 2 wt. % catalyst was charged. The NO conversion increased sharply to approximately 57% when the powder catalyst corresponding to 3 wt. % was charged. These results mean

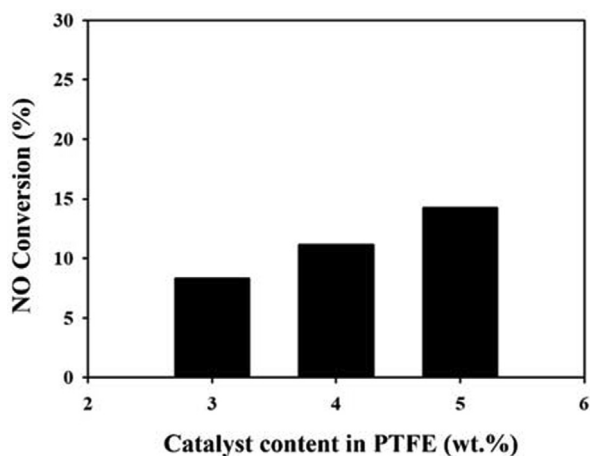


Fig. 14. NO conversion by NH_3 -SCR reaction at 200 °C on PTFE-based catalytic filter prepared with a mixing content of $\text{V}_2\text{O}_5(2.5)$ - $\text{MnO}_2(7.5)$ /USY-zeolite catalyst.

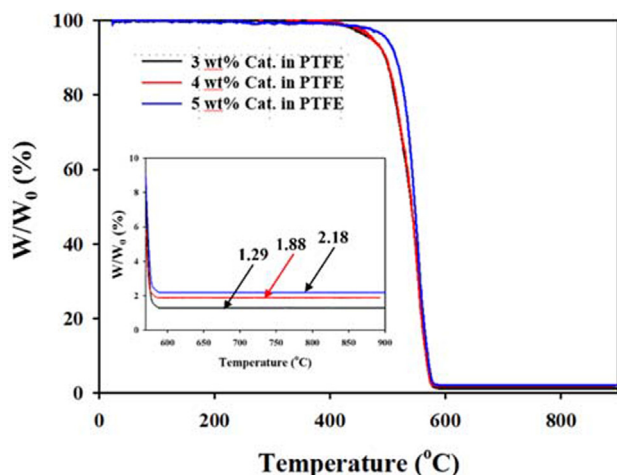


Fig. 15. TGA results of PTFE fiber containing 3.0, 4.0, and 5.0 wt. % of $\text{V}_2\text{O}_5(2.5)$ - $\text{MnO}_2(7.5)$ /USY-zeolite catalysts under air-flow conditions.

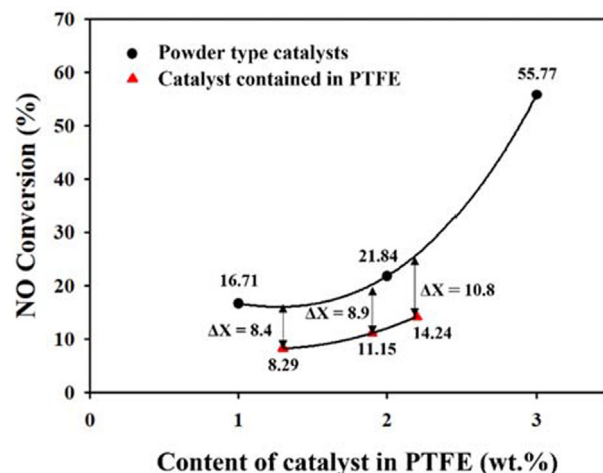


Fig. 16. NO conversion by NH_3 -SCR reaction at 200 °C on powder type $\text{V}_2\text{O}_5(2.5)$ - $\text{MnO}_2(7.5)$ /USY-zeolite catalysts corresponding to the content of catalysts contained in the PTFE catalytic filter.

that maintaining the impregnation amount of catalyst above 3 wt. % in the PTFE fiber can achieve a high NO conversion which is comparable to a powder-type catalyst. On the other hand, the performance of approximately 8.3, 11.2, and 14.2% was maintained when the catalyst in the PTFE catalytic fiber shown in Fig. 15 contained approximately 1.3, 1.9, and 2.2 wt.%, respectively. Therefore, approximately 49.5, 55.6 and 56.8% of the performance of the powder catalysts was obtained when the catalyst was impregnated in the PTFE fiber. From these results, the catalyst particles entangled inside PTFE polymer fiber cannot be used as a catalyst due to gas diffusion resistance. Only the catalyst exposed on the external surface of PTFE fiber can be used for the NH_3 -SCR reaction. It can be concluded that approximately 50–57% of the catalysts added to PTFE was present on the external surface of the PTFE fibers, and the remaining fine particles were buried in the fibers.

Conclusion

This study prepared catalyst-embedded PTFE fibers to remove low-concentration NO_x and dust collection in a bag filter. In the previous study, catalytic filters were produced by coating the catalyst on the surface of the filter. However, since PTFE-based fibers are hydrophobic fluorine-based polymer fibers, an organic solvent is needed to coat the powder catalyst on the PTFE fiber. In addition, the coated catalyst can be easily separated from the bag filter during the backwashing process due to the weak interaction between catalyst powder and fiber. In this study, a catalyst was pre-added during the fiber manufacturing process to produce a uniform dispersion in the PTFE fiber. A high surface area and hydrophobic USY-based zeolite were used as a catalytic support material to improve the catalytic activity for reducing low concentration of NO in the exhaust gas. In addition, V_2O_5 and MnO_2 were used as catalytically active materials to obtain high activity at a low temperature in the bag filter process. The catalytic activity of V_2O_5 - MnO_2 /USY-based zeolite for NH_3 -SCR reaction was enhanced due to the strong NH_3 adsorption strength on MnO_2 . The ratio of V_2O_5 to MnO_2 contained in the catalyst was optimized to minimize the catalytic deactivation by SO_2 poisoning. The prepared catalyst was embedded in the PTFE fibers by pre-mixing catalyst and PTFE powder before being compressed. The amount of catalyst contained in the PTFE catalytic fiber was confirmed to be approximately 43% of the amount added. A considerable amount of catalyst loss occurs in manufacturing the fibers by slitting the PTFE film. In addition, the NH_3 -SCR performance of the PTFE catalytic

fiber was approximately 60% of that of the powder catalyst corresponding to the same catalyst. This is because the fine catalyst particles inside the PTFE fibers do not come into contact with the exhaust gas. Nevertheless, considerable catalytic activity was observed due to the formation of valleys on the fiber surface and the migration of catalyst particles during the rolling and stretching process of the PTFE rod. High NO_x removal performance is expected if the actual catalyst content in the PTFE fiber is more than 3 wt. %. Finally, the catalyst could be added uniformly to the PTFE fibers. Therefore, catalyst-embedded PTFE fibers can be used for the removal of nitrogen oxides and dust as raw materials of the bag filter.

Declaration of Competing Interest

The authors declare that they have no known competing financial interests or personal relationships that could have appeared to influence the work reported in this paper.

Acknowledgment

This work was supported by Korea Environment Industry & Technology Institute (KEITI) through The Reduction Management Program of Fine Dust Blind-Spots Project, funded by the Korea Ministry of Environment (MOE) (2020003060007).

Reference

- R.A. VanCuren, T.A. Cahill, J. Geophys. Res. 107 (D24) (2002) 4804. <http://doi.org/10.1029/2002JD002204>.
- A. Malaguti, M. Mircea, T.M.G. La Torretta, C. Telloli, E. Petralia, M. Stracquadanio, M. Berico, Aerosol Air Qual. Res. 15 (2015) 410–425. <http://doi.org/10.4209/aaqr.2014.08.0172>.
- Y.Y. Xu, Y. Zhang, J. Wang, J.Q. Yuan, Engineering 49 (2013) 50–60. <https://doi.org/10.1016/j.compchemeng.2012.09.014>.
- D. Pudasainee, J.-H. Kim, Y.-S. Yoon, Y.-C. Seo, CS-ESP and wet FGD, Fuel 93 (2012) 312–318. <https://doi.org/10.1016/j.fuel.2011.10.012>.
- R. Stolle, H. Koesse, H. Gutberlet, Appl Catal B 144 (2014) 486–497. <https://doi.org/10.1016/j.apcatb.2013.07.040>.
- S.A. Benson, J.D. Laumb, C.R. Crocker, J.H. Pavlish, Fuel Process. Technol. 86 (5) (2005) 577–613. <https://doi.org/10.1016/j.fuproc.2004.07.004>.
- K. Nakamura, T. Muramatsu, T. Ogawa, T. Nakagaki, Energy 227 (2021) 120383–120392. <https://doi.org/10.1016/j.energy.2021.120383>.
- X. Ke, R. Cai, M. Zhang, M. Miao, J. Lyu, H. Yang, Fuel Process. Technol. 181 (2018) 252–258. <https://doi.org/10.1016/j.fuproc.2018.10.001>.
- R.K. Srivastava, W. Neuffer, D. Grano, S. Khan, J.E. Staudt, W. Jozewicz, Environ. Prog. 24 (2) (2005) 181–197. <https://doi.org/10.1002/ep.10063>.
- X.-Z. Feng, O. Lugovoy, H. Qin, Adv. Clim. Chang. Res. 9 (1) (2018) 34–42. <https://doi.org/10.1016/j.accre.2018.02.004>.
- S.M. Jeong, S.D. Kim, Korean J. Chem. Eng. 16 (5) (1999) 614–617. <http://doi.org/10.1007/BF02708140>.
- B.S. Kim, T.Y. Kim, T.C. Park, Y.K. Yeo, Korean J. Chem. Eng. 35 (9) (2018) 1779–1790. <http://doi.org/10.1007/s11814-018-0087-8>.
- J.S. Cha, S.H. Park, J.-K. Jeon, Y.-K. Park, Appl. Chem. Eng. 22 (4) (2011) 433–438.
- L.J. Muzio, G.C. Quartucy, J.E. Cichanowicz, Int. J. Environ. Pollut. 17 (1–2) (2002) 4–30. <https://doi.org/10.1504/IJEP.2002.000655>.
- J.V. Canneghem, J. De Greef, C. Block, C. Vandecasteele, J. Clean. Prod. 112 (5) (2016) 4452–4460. <https://doi.org/10.1016/j.jclepro.2015.08.068>.
- S.-W. Choi, S.-K. Choi, H.-K. Bae, J. Air Waste Manag. Assoc. 65 (4) (2015) 485–491. <https://doi.org/10.1080/10962247.2014.1002584>.
- A. Grossale, I. Nova, E. Tronconi, D. Chatterjee, M. Weibel, J. Catal. 256 (2) (2008) 312–322. <https://doi.org/10.1016/j.jcat.2008.03.027>.
- M.P. Ruggeri, T. Selli, M. Colombo, I. Nova, E. Tronconi, J. Catal. 311 (2014) 266–270. <https://doi.org/10.1016/j.jcat.2013.11.028>.
- J.-K. Lai, I.E. Wachs, ACS Catal. 8 (2018) 6537–6551. <https://doi.org/10.1021/acscatal.8b01357>.
- B. Wang, Z. Song, L. Sun, Chem. Eng. J. 409 (2021) 128136–128155. <https://doi.org/10.1016/j.cej.2020.128136>.
- J. Hwang, H.-J. Ha, J. Ryu, J.-J. Choi, C.-W. Ahn, J.-W. Kim, B.-D. Hahn, W.-H. Yoon, H. Lee, J.-H. Choi, Catal. Commun. 94 (2017) 1–4. <https://doi.org/10.1016/j.jcatcom.2017.02.002>.
- T. Schwammle, F. Bertsche, A. Hartung, J. Brandenstein, B. Heidel, G. Scheffknecht, Chem. Eng. J. 222 (2013) 274–281. <https://doi.org/10.1016/j.cej.2013.02.057>.
- Z. Lei, X. Liu, M. Jia, Energy & Fuel 23 (2009) 6146–6151. <http://doi.org/10.1021/ef900713y>.
- K. Li, J. Jin, K. Li, R. Wu, H. Zhang, Mater. Res. Express 8 (2021). <https://doi.org/10.1088/2053-1591/ac1aaa>.
- S. Heidenreich, M. Nacken, M. Hackel, G. Schaub, Powder Technol. 180 (1–2) (2008) 86–90. <https://doi.org/10.1016/j.powtec.2007.02.033>.
- R. Wu, J. Jin, K. Li, L. Zhao, H. Zhang, Mater. Res. Express 8 (2021). <https://doi.org/10.1088/2053-1591/abfa48>.
- M. Nacken, S. Heidenreich, M. Hackel, G. Schaub, NO_x removal and VOC total oxidation, Applied Catalysis B: Environmental 70 (1–4) (2007) 370–376. <https://doi.org/10.1016/j.apcatb.2006.02.030>.
- J.-H. Choi, S.-K. Kim, Y.-C. Bak, Korean J. Chem. Eng. 18 (2001) 719–724.
- K. Li, T. Zhou, X. Xu, C. Han, H. Zhang, J. Jin, Sustainability 14 (9) (2022) 5353. <https://doi.org/10.3390/su14095353>.
- K.J. Fritsky, H.H. Kumm, M. Wilken, J. Air Waste Manag. Assoc. 51 (2001) 1642–1649. <https://doi.org/10.1080/10473289.2001.10464391>.
- J.L. Bonte, K.J. Fritsky, M.A. Plinke, M. Wilken, Waste Manag. 22 (4) (2002) 421–426. [https://doi.org/10.1016/S0956-053X\(02\)00025-9](https://doi.org/10.1016/S0956-053X(02)00025-9).
- E. Finocchio, G. Busca, M. Notaro, Appl Catal B 62 (1–2) (2006) 12–20. <https://doi.org/10.1016/j.apcatb.2005.06.010>.
- C. Chen, Y. Cao, S. Liu, J. Chen, W. Jia, Chin. J. Catal. 39 (8) (2018) 1347–1365. [https://doi.org/10.1016/S1872-2067\(18\)63090-6](https://doi.org/10.1016/S1872-2067(18)63090-6).
- J. Zhang, X. Li, P. Chen, B. Zhu, Materials 11 (9) (2018) 1632. <https://doi.org/10.3390/ma11091632>.
- C. Xu, J. Liu, Z. Zhao, F. Yu, K. Cheng, Y. Wei, A. Duan, C. Jiang, J. Environ. Sci. 31 (2015) 74–80. <https://doi.org/10.1016/j.jes.2014.09.040>.
- Z. Zhao, E. Li, Y. Qin, X. Liu, Y. Zou, H. Wu, T. Zhu, Journal of Environmental Science 90 (2020) 119–137. <https://doi.org/10.1016/j.jes.2019.11.008>.
- P. Wu, K. Shen, Y. Liu, Y. Zhang, G. Li, H. Yang, S. Wang, Cat. Sci. Technol. 11 (2021) 4115–4132. <https://doi.org/10.1039/D1CY00227A>.
- L. Wei, R. Guo, J. Zhou, X. Chen, Z. Bi, W. Pan, Fuel 316 (2022). <https://doi.org/10.1016/j.fuel.2022.123438>.
- C. Liu, J.-W. Shi, C. Gao, C. Niu, Appl. Catal. A 522 (2016) 54–69. <https://doi.org/10.1016/j.apcata.2016.04.023>.
- D. Fang, J. Xie, H. Hu, H. Yang, F. He, Z. Fu, Chem. Eng. J. 271 (2015) 23–30. <https://doi.org/10.1016/j.cej.2015.02.072>.
- G. Xu, X. Guo, X. Cheng, J. Yu, B. Fang, Nanoscale 13 (2021) 7052–7080. <https://doi.org/10.1039/D1NR00248A>.
- A. Sultana, M. Sasaki, H. Hamada, Catal. Today 185 (1) (2012) 284–289. <https://doi.org/10.1016/j.cattod.2011.09.018>.
- S. Yang, F. Qi, S. Xiong, H. Dang, Y. Liao, P.K. Wong, J. Li, Appl Catal B 181 (2016) 570–580. <https://doi.org/10.1016/j.apcatb.2015.08.023>.
- K. Guo, J. Ji, W. Song, J. Sun, C. Tang, L. Dong, Appl Catal B 297 (2021). <https://doi.org/10.1016/j.apcatb.2021.120388>.
- Y. Zhu, Q. Hou, M. Shreka, L. Yuan, S. Zhou, Y. Feng, C. Xia, Catalysts 9 (1) (2019) 21. <https://doi.org/10.3390/catal9010021>.
- J. Meng, Y. Duan, P. Hu, Y. Xu, X. Geng, T. Yao, S. Ren, H. Wei, Energy Fuel 33 (2019) 8896–8906. <https://doi.org/10.1021/acs.energyfuels.9b01503>.
- X. Tang, J. Hao, H. Yi, J. Li, Catal. Today 126 (3–4) (2007) 406–411. <https://doi.org/10.1016/j.cattod.2007.06.013>.
- X. Zhao, L. Huang, H. Li, H. Hu, J. Han, L. Shi, S. Zhang, Chin. J. Catal. 35 (11) (2015) 1886–1899. [https://doi.org/10.1016/S1872-2067\(15\)60958-5](https://doi.org/10.1016/S1872-2067(15)60958-5).
- L. Jiang, Q. Liu, G. Ran, M. Kong, S. Ren, J. Yang, J. Li, Chem. Eng. J. 370 (2019) 810–821. <https://doi.org/10.1016/j.cej.2019.03.225>.
- M. Musil, B. Choi, A. Tsutsumi, J. Electrochem. Soc. 162 (10) (2015) A2058–A2065. <https://doi.org/10.1149/2.0201510jes>.
- W. Wang, Y. Kan, B. Yu, Y. Pan, K.M. Liew, L. Song, Y. Hu, Compos. A 95 (2017) 173–182. <https://doi.org/10.1016/j.compositesa.2017.01.009>.
- B.M. Reddy, B. Chowdhury, I. Ganesh, E.P. Reddy, T.C. Rojas, A. Fernandez, J. Phys. Chem. B 102 (1998) 10176–10182. <https://doi.org/10.1021/jp9826165>.
- G. Silversmit, D. Depla, H. Poelman, G.B. Marin, R. De Gryse, Surf. Sci. 600 (2006) 3512–3517. <http://doi.org/10.1016/j.susc.2006.07.006>.
- H.W. Nesbitt, D. Banerjee, Am. Mineral. 83 (1998) 305–315. <http://doi.org/10.2138/am-1998-3-414>.
- J.M. de O. Cremonizzi, D.Y. Tiba, S.H. Domingues, SN Applied Sciences 2 (2020) 1689. <https://doi.org/10.1007/s42452-020-03488-2>.
- M. Wark, M. Koch, A. Bruckner, W. Grunert, J. Chem. Soc., Faraday Trans. 94 (14) (1998) 2033–2041. <https://doi.org/10.1039/A800522B>.
- J.-H. Park, S.-H. Jeon, N. Van Khoa, C.-H. Shin, Clean Technology 15 (2) (2009) 122–129.
- Siddharth, S. Maiti, H. Haj, R. S. Bisht, A. K. Minocha, S. K. Panigrahi, S. Alexander, Materials Research Express, 5, 085507 (2018). <http://doi.org/10.1088/2053-1591/aad2e9>.
- B. Talukdar, H.M. Meyer III, C. Mukarakata, K. Iisa, M.B. Griffin, S.E. Jabas, K.A. Unocic, Microsc. Microanal. 28 (Suppl 1) (2022) 2472–2474. <http://doi.org/10.1017/S1431927622009461>.
- S. Wang, R. Guo, W. Pan, Q. Chen, P. Sun, M. Li, S. Liu, Catal. Commun. 89 (2017) 143–147. <https://doi.org/10.1016/j.catcom.2016.11.005>.
- F. Liu, H. He, C. Zhang, W. Shan, X. Shi, Catal. Today 175 (2011) 18–25. <https://doi.org/10.1016/j.cattod.2011.02.049>.
- W. Li, R. Guo, S. Wang, W. Pan, Q. Chen, M. Li, P. Sun, S. Liu, Fuel Process. Technol. 154 (2016) 235–243. <https://doi.org/10.1016/j.fuproc.2016.08.038>.
- B. Zhang, S. Zhang, B. Liu, H. Shen, L. Li, The Royal Society of Chemistry Advances 8 (2018) 12733–12741. <https://doi.org/10.1039/c8ra00336j>.
- X. Yao, T. Kong, S. Yu, L. Li, F. Yang, L. Dong, Appl. Surf. Sci. 402 (2017) 208–217. <https://doi.org/10.1016/j.apsusc.2017.01.081>.
- N. Zhang, L. Li, B. Zhang, Y. Sun, L. Song, R. Wu, H. He, J. Environ. Chem. Eng. 7 (3) (2019). <https://doi.org/10.1016/j.jece.2019.103044>.